

Force Control of Musculoskeletal Manipulator Driven By Spiral Motors

DOI 10.7305/automatika.54-1.307
UDK 681.532-531.8:612.7; 531.1
IFAC 3.2; 1.2.2

Original scientific paper

This paper presents force control of musculoskeletal manipulator driven by spiral motors. The kinematic and dynamic properties are shown to address the presence of environmental contact with the manipulator. From this contact, the force control schemes were explored, by comparing between monoarticular-only structure and biarticular structure manipulator. Force control schemes were divided into independent muscle control, end effector step force command, and muscular viscoelasticity control. The results show advantages of biarticular actuation compared to monoarticular-only actuation in the feasibility of magnetic levitation (gap) control alongside force control.

Key words: biarticular muscle, force control, closed kinematic, parallel manipulator, muscular viscoelasticity

Upravljanje silom mišićno-koštanog manipulatora pogonjenog spiralnim motorom. U ovome radu predstavljeno je upravljanje silom mišićno-koštanog manipulatora pogonjenog spiralnim motorom. Kinematička i dinamička svojstva prikazuju prisutnost kontakta manipulatora s okolinom. Na temelju kontakta istraženo je upravljanje silom usporedbom jednozglobne i dvozgladne strukture manipulatora. Upravljanje silom podijeljeno je u neovisno upravljanje mišićima, upravljanje alatom manipulatora (eng. *end effector*) i upravljanje mišićnom viskoelastičnosti. Rezultati pokazuju prednost dvozgladne strukture u odnosu na jednozglobnu u smislu izvedivosti upravljanja magnetskom levitacijom pored upravljanja silom.

Ključne riječi: dvozglodna struktura mišića, upravljanje silom, zatvorena kinematika, paralelni manipulator, mišićna viskoelastičnost

1 INTRODUCTION

Current implementation of mobile human-biologically-inspired robots can be seen in a variety of successful designs such as Humanoid Honda ASIMO [1], DLR robot arms [2], BigDog [3] and others. These designs have shown high manipulability, mobility, compliance and ability to perform various tasks previously deemed as very difficult for a machine. The success is mainly attributed to the successful design and control of joint servo motors at the hinges, i.e. elbows, shoulders, knees and ankles. Although the use of joint servo motors is sufficient for current tasks, problems such as friction, backlash due to the use of gears and mechanisms are not negligible. Thus, researchers started venturing into direct drive actuators. However, the design of direct-drive joint actuators increases the weight of the motors.

A direct drive system for robotic systems, was reported in [4]. It avoids friction loss and realizes good controllability. Also, sensorless force control based on disturbance observer was shown in [5]. However, problems of mass and

volume of the robot arise (i.e. become large). Another sensorless force control of manipulator with geared robots was presented in [6]. The bandwidth of the system was limited to gear friction. One of the solutions to improve force control system was to combine accelerometer with disturbance observer [7] by enhancing sensing bandwidth. Another solution was to implement a twin-drive system which cancels the static friction of the two geared motors via differential gear system [8]. Some actuators utilize elastic actuators between the output and gears [9] [10]. Although improving stability and safety, high frequency domain controllability is reduced.

The actual musculoskeletal structure of humans inspired several researchers to focus on the use of actuators to represent the muscles attached to the skeleton. The unique feature of the human arm is the existence of the antagonistic pairs of muscles on the joints, and the usage of biarticular muscles for motion. Pneumatic muscle actuators are arguably similar to the actual human muscles, as shown by some researchers [11] - [14]. The pneu-

matic muscles can be placed very near the skeleton structure. However, the use of air supply could reduce mobility. Also, fast and stable control of such actuators [15] is difficult to achieve compared to electrical motors. Some researchers use hydraulic actuators such as the HyQ robot [16] and exoskeleton XOS [17].

Some biarticular arm designs using electrical actuation have also been researched [18] [19]. In [18], the design uses electrical motors alongside mechanisms (pulley, gears) to actuate monoarticular and biarticular actuators. As such, biarticular forces were viewed from joint angle perspective, without any closed-chain kinematics. Stiffness, feedforward inverse dynamics control was applied. For the Bi-Articularly Actuated and Wire Driven Robot Arm [19], the muscles were represented by wires for actuation. By pulling or releasing the wires, 6 antagonistic muscles can be actuated using 6 servo motors. Force redundancy was solved using the infinity norm approach. In another research [20], virtual triarticular muscle control (with properties of AC motor control) was used to control the Lancelet robot (inspired from the ancestor of the vertebrae). The robot emulated swimming motion using the virtual triarticular muscle control.

Focusing on prismatic/translational/linear actuators, many works on PM linear synchronous motors have been reported. In [21], a high thrust density linear motor (HDL) has been proposed. HDL generates thrust force two times larger than linear induction motors. Tubular linear permanent magnet (TLPM) motors suggest practicality because of direct-drive motion and elimination of mechanical transmission losses [22]. An application example of TLPM is for drilling [23] and elevator door [24]. In general, by providing current control in the stator of these motors, tube-shaped movers (with Permanent Magnets) are levitated and then direct drive motion can be realized.

Currently, in our laboratory, a new direct-drive translational actuator, the spiral motor has been developed. The first prototype of a new spiral motor (of helical structure) which is direct drive, high backdrivable, high output ratio was shown in [25]. From the first prototype, the internal permanent version was developed and lately, the surface permanent magnet prototype [26] [27] for this research. The basic idea is that these spiral motors represent the muscles, one for each pair of antagonistic muscles, i.e. one spiral motor for shoulder monoarticulars, one spiral motor for elbow monoarticulars and one spiral motor for the biarticular muscles. The reason behind this is because the spiral motor is a high force density, high forward and backward drivable actuator, i.e. equal forces can be applied in forward or reverse direction.

1.1 Research Focus

The monoarticular and biarticular muscles are retained in its linear form, by using spiral motors. In [28], we have shown some probable position control schemes of the biarticular manipulator. In this paper, the focus is to address force control on the biarticular manipulator structure at the end effector, and also apply muscular viscoelasticity control. The purpose of simulating different force control schemes is to estimate the feasibility and safety of magnetic levitation of the spiral motor. Proper control will not only enable direct drive but also compliance.

1.2 Organization of Paper

This paper is organized as follows; Section 2 describes the geometrical analysis of the biarticular structure, Section 3 introduces the spiral motor, Section 4 shows gap control on musculoskeletal configuration, Section 5 shows the biarticular dynamics model with environmental constraints and Section 6 describes the force control schemes for the biarticular manipulator.

2 BIARTICULAR MUSCLE STRUCTURE

The human arm is an obvious biarticular structure, consisting of monoarticular and biarticular muscles attached to certain points of the arm bones. The combined flexor/extensor muscles of the planar manipulator of the biarticular structure is shown in Fig. 1. Based on Fig. 1 and using trigonometric identities, the relationship of muscle lengths, l_m with joint angles q is derived as in (1).

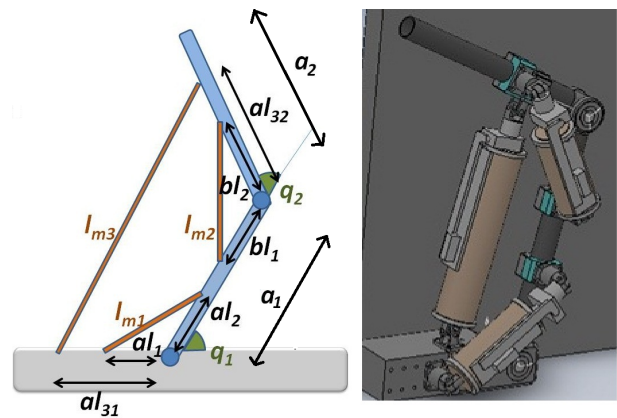


Fig. 1. Biarticular structure (sketch and Solidworks model)

$$l_m = \begin{bmatrix} l_{m1} \\ l_{m2} \\ l_{m3} \end{bmatrix} \quad (1)$$

where

$$\begin{aligned}
l_{m1} &= \sqrt{al_1^2 + al_2^2 + 2al_1al_2\cos q_1} \\
l_{m2} &= \sqrt{bl_1^2 + bl_2^2 + 2bl_1bl_2\cos q_2} \\
l_{m3} &= \{al_{31}^2 + al_{32}^2 + a_1^2 \\
&\quad + 2al_{31}a_1\cos q_1 \\
&\quad + 2al_{32}a_1\cos q_2 \\
&\quad + 2al_{31}al_{32}\cos(q_1 + q_2)\}^{1/2} \quad (2)
\end{aligned}$$

It is apparent that the extension or contraction of monoarticular muscles affect the respective joint angles to which they attach, i.e. muscle 1 affects the joint angle q_1 and muscle 2 affects the joint angle q_2 . However, the biarticular muscle 3 is redundant, because it affects both joint angles.

Based on (1) and (2), the relation between muscle velocity and joint velocity is given as in (3).

$$\dot{l}_m = J_{lmq} \dot{q} \quad (3)$$

where J_{lmq} is the Jacobian matrix between muscle and joint space and contains the following elements.

$$J_{lmq} = \begin{bmatrix} \frac{\partial l_{m1}}{\partial q_1} & \frac{\partial l_{m1}}{\partial q_2} \\ \frac{\partial l_{m2}}{\partial q_1} & \frac{\partial l_{m2}}{\partial q_2} \\ \frac{\partial l_{m3}}{\partial q_1} & \frac{\partial l_{m3}}{\partial q_2} \end{bmatrix} \quad (4)$$

Hence, the elements of the Jacobian matrix are derived.

$$\begin{aligned}
\frac{\partial l_{m1}}{\partial q_1} &= \frac{al_1al_2\sin q_1}{l_{m1}}; & \frac{\partial l_{m1}}{\partial q_2} &= 0 \\
\frac{\partial l_{m2}}{\partial q_1} &= 0; & \frac{\partial l_{m2}}{\partial q_2} &= \frac{bl_1bl_2\sin q_2}{l_{m2}} \\
\frac{\partial l_{m3}}{\partial q_1} &= \frac{-al_{31}a_1\sin q_1 - al_{31}al_{32}\sin(q_1 + q_2)}{l_{m3}} \\
\frac{\partial l_{m3}}{\partial q_2} &= \frac{-al_{32}a_1\sin q_2 - al_{31}al_{32}\sin(q_1 + q_2)}{l_{m3}} \quad (5)
\end{aligned}$$

Thus, the equation relating joint torques τ (vector of q_1 and q_2) and muscle forces F_{lm} (vector of l_{m1} , l_{m2} and l_{m3}) can be described.

$$\tau = J_{lmq}^T F_{lm} \quad (6)$$

Also, the equation relating the joint torque and the end effector force, F_e (vector of cartesian forces) for a two link planar rotary manipulator is shown in (7).

$$\tau = J^T F_e \quad (7)$$

where J is the Jacobian matrix from the task space to the joint space and contains the following elements.

$$\begin{bmatrix} -a_1\sin(q_1) - a_2\sin(q_1 + q_2) & -a_2\sin(q_1 + q_2) \\ a_1\cos(q_1) + a_2\cos(q_1 + q_2) & a_2\cos(q_1 + q_2) \end{bmatrix} \quad (8)$$

The relationship between the end effector forces and the muscle forces can be determined as follows.

$$F_e = [J^T]^{-1} J_{lmq}^T F_{lmq} \quad (9)$$

One of the advantages of actuation redundancy of biarticular manipulator is the force ellipsoid, which is hexagon in shape, compared to tetragon for non-biarticular manipulators [29].

3 THE SPIRAL MOTOR

The spiral motor is a novel high thrust force actuator with high backdrivability, consists of a helical structure mover and stator with permanent magnet. The mover moves spirally in the stator, and the linear motion is extracted to drive the load. Thus, the motor realizes direct-drive motion. Moreover, the motor has high thrust-force characteristics because the flux is effectively utilized in its 3-D structure [25]. The illustration and assembled spiral motor are shown in Fig. 2 and Fig. 3.

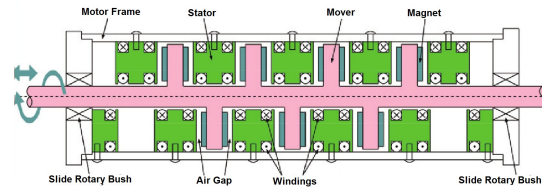


Fig. 2. Spiral Motor Illustration

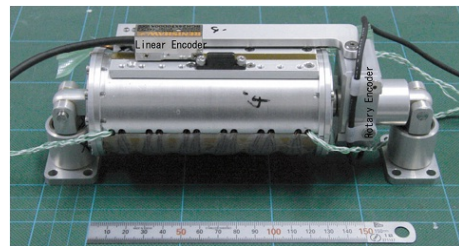


Fig. 3. Assembled Short-stroke Spiral Motor

The spiral motor has two degree-of-freedom (dof) control. By controlling the small air gap between the mover and stator, magnetic levitation is realized. Then, the angular control provided by q-axis current will give forward or backward thrust. The main advantage of the spiral motor is capability of direct drive frictionless motion. The spiral motor equations of motions can be described in (10) to (13).

$$M_s \ddot{x} = K_f I_d + K_g x_g - d_x \quad (10)$$

$$J_s \ddot{\theta} = K_\tau I_q - h(K_f I_d + K_g x_g) - d_\theta \quad (11)$$

$$x_g = x - h\theta \quad (12)$$

$$h = \frac{l_p}{2\pi} \quad (13)$$

$M_s \ddot{x}$ is the thrust of the spiral motor with M_s as mass, $J_s \ddot{\theta}$ is the spiral motor torque with J_s as inertia, $K_f I_d$ is the force from d- axis current and $K_\tau I_q$ is the force from q-axis current, $K_g x_g$ represents the force generated during magnetic levitation (x_g is the gap between mover and stator) and l_p is lead length of screw. Gap displacement x_g is related to linear, x and angular displacement, θ . Linear and angular disturbances are labelled d_x and d_θ .

4 GAP CONTROL ON MUSCULOSKELETAL STRUCTURE

The direct drive control of spiral motors without attaching it to any structure has been shown previously in [27]. This was due to the success of maintaining two degrees of freedom control, which is magnetic levitation (gap) and rotational motion (θ) to realize forward and backward strokes. However, in the previous setup, the actuator is free to move without any constraints on the mover/stator attachments.

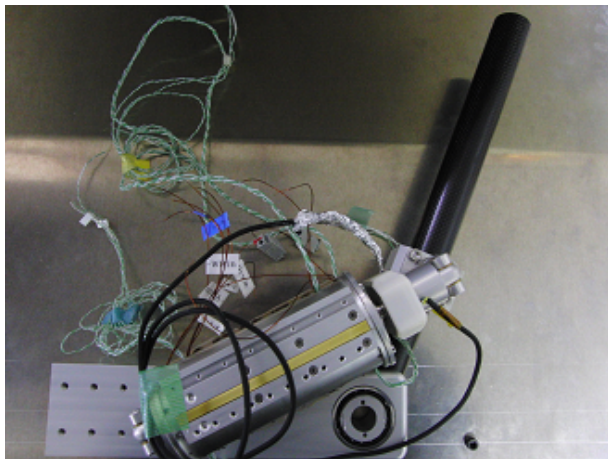


Fig. 4. Structure of musculoskeletal actuation: Shoulder monoarticular

In Fig. 4, we attach the 60mm stroke spiral motor to the manipulator configuration. Note the position of the motor, which is intended to emulate monoarticular actuation. Gap control is essential in the direct-drive motion of the spiral motor because if motion is performed without gap control, there would be large frictional forces between the

mover and stator, The gap starts from touch down (contact with stator) offset position. Then magnetic levitation is performed so that stator and mover do not contact.

For vector control of spiral motor, the control variables for gap and angular terms are shown.

$$u_{xg} = K_{pg}(x_{gref} - x_g) + K_{dg}(\dot{x}_{gref} - \dot{x}_g) \quad (14)$$

$$u_\theta = K_{pt}(\theta_{ref} - \theta) + K_{dt}(\dot{\theta}_{ref} - \dot{\theta}) \quad (15)$$

The spiral motor thrust dynamics in terms of gap and angle are shown next.

$$M_s \ddot{x} = M_s(\ddot{x}_g + h\ddot{\theta}) = K_f I_d + K_g x_g - d_x \quad (16)$$

However, this time we will use only d-axis current to control the gap. Thus d-axis current reference can be derived by matching the gap control variable with the gap acceleration in the spiral motor dynamics ($M_n, K_{gn}, K_{\tau n}$ are controller-assigned mass, gap constant, thrust constant values for spiral motor and \hat{d}_{xg} is the gap disturbance estimation term).

$$I_{dref} = \frac{1}{K_{\tau n}}(M_n(u_{xg}) - K_{gn}x_g + \hat{d}_{xg}) \quad (17)$$

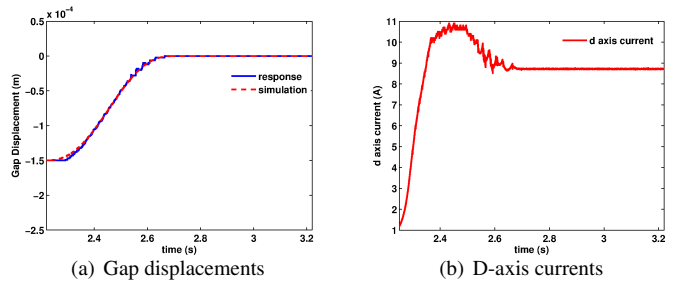


Fig. 5. Gap levitation at -150 um offset

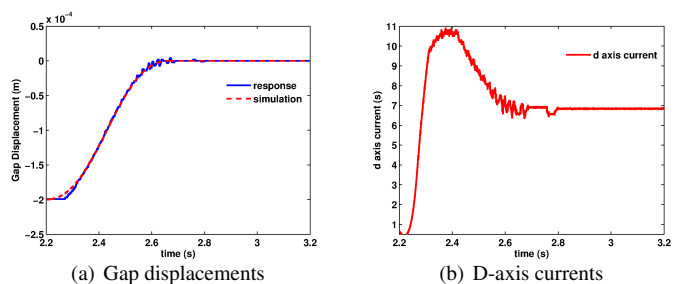


Fig. 6. Gap levitation at -200 um offset

Figures 5 to 7 show the experimental results of gap displacements with different initial values for gap. The actual

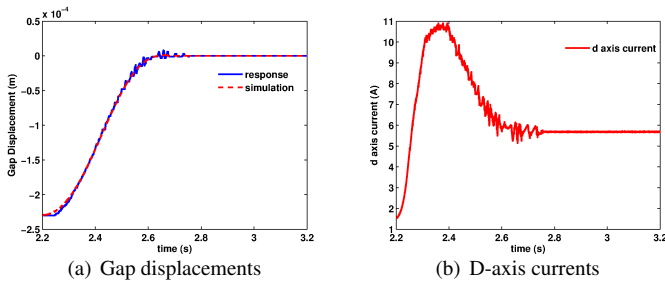


Fig. 7. Gap levitation at -230 μm offset

gap values within the stator are unknown, but can be estimated via linear and rotational sensors. Deformations can be caused from irregular surface of mover and/or stator.

The experimental results show that magnetic levitation was achieved for the monoarticular structure and the gap in the initial position of the actuator has at least 230 μm space. In the results, the larger the initial gap offset value, the lesser d-axis current is required to maintain the gap at steady state. For direct drive motion (i.e. force or position control) combination of d and q-axis currents will have to be controlled simultaneously. This initial stage of gap stabilization is very important and experiments show the feasibility of gap control. Without stable gap control, magnets on the rotor will hit the stator blocks. Base on our experience, too much collision and heat will cause the teeth of the yokes to be broken. The initial stage of force control in Section 6 prior to 0.5 s is magnetic levitation (gap) control.

5 BIARTICULAR DYNAMICS MODEL WITH ENVIRONMENTAL CONSTRAINTS

For a two-link planar rotary manipulator, the dynamic equations of motion would incur the use of Ordinary Differential Equation of the following generalized form with M as inertia/mass matrix, C as Centrifugal/Coriolis, g as gravity terms, τ as generalized torques/forces.

$$M(q)\ddot{q} + C(q, \dot{q})\dot{q} + g(q) = \tau \quad (18)$$

For a biarticular manipulator, due to its closed-kinematic chain, the dynamics would require an additional term [30] [31], λ is Lagrange multiplier and J_c is the Jacobian of the constraint equation(s) as shown in (19). This combined term is the vector of constraint forces.

$$M(q)\ddot{q} + C(q, \dot{q})\dot{q} + g(q) = \tau + J_c^T \lambda \quad (19)$$

Firstly, the closed-chain system is virtually cut open at the connection point between the muscles (mover end) and the links. Then, the 'open-chain' terms are derived using Lagrange-Euler formulation. The inertia matrix

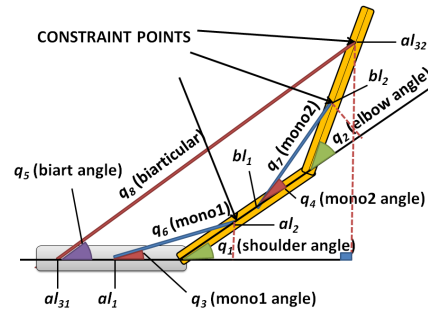


Fig. 8. Illustration of Biarticular Constraints

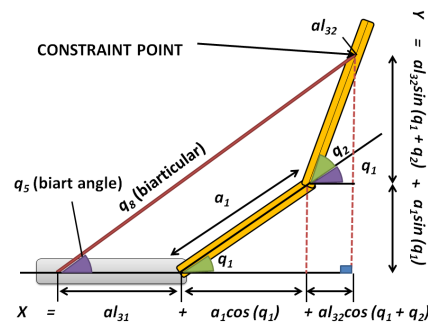


Fig. 9. Biarticular Link Constraint in XY coordinates

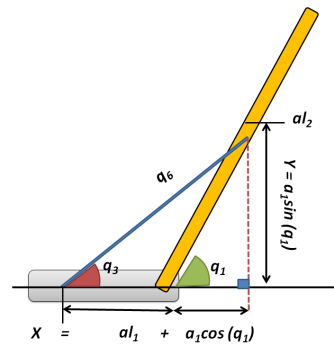


Fig. 10. Monoarticular Link Constraint in XY coordinates

terms were obtained from the Jacobians and the Coriolis/Centrifugal terms computed from Christofel symbols [32]. Gravity is ignored as this setup is intended to be in planar configuration.

Also, the relative acceleration at the constraint is zero (J_c is constraint Jacobian and \dot{J}_c is constraint Jacobian derivative),

$$J_c \ddot{q} + \dot{J}_c \dot{q} = 0 \quad (20)$$

The Jacobian of the constraints (J_c) can be obtained by partial differentiation of the six constraint equations (in X and Y, see Figs 8 to 10) with respect to the 8 link variables.

Unmentioned terms are zero.

$$\begin{aligned}
 J_{c11} &= a l_2 \sin(q_1) \\
 J_{c13} &= -q_6 \sin(q_3) \\
 J_{c16} &= \cos(q_3); \\
 J_{c21} &= -a l_2 \cos(q_1) \\
 J_{c23} &= q_6 \cos(q_3) \\
 J_{c26} &= \sin(q_3) \\
 J_{c32} &= b l_2 \sin(q_2) \\
 J_{c34} &= -q_7 \sin(q_4) \\
 J_{c37} &= \cos(q_4); \\
 J_{c42} &= -b l_2 \cos(q_2) \\
 J_{c44} &= q_7 \cos(q_4) \\
 J_{c47} &= \sin(q_4) \\
 J_{c51} &= a l_{32} \sin(q_1 + q_2) + a_1 \sin(q_1) \\
 J_{c52} &= a l_{32} \sin(q_1 + q_2) \\
 J_{c55} &= -q_8 \sin(q_5) \\
 J_{c58} &= \cos(q_5) \\
 J_{c61} &= -a l_{32} \cos(q_1 + q_2) - a_1 \cos(q_1) \\
 J_{c62} &= -a l_{32} \cos(q_1 + q_2) \\
 J_{c65} &= q_8 \cos(q_5) \\
 J_{c68} &= \sin(q_5)
 \end{aligned} \tag{21}$$

The Jacobian time derivatives (\dot{J}_c) of the constraints are derived by differentiating the constraint Jacobian with respect to time.

$$\begin{aligned}
 J_{d11} &= a l_2 \cos(q_1) \dot{q}_1 \\
 J_{d13} &= -q_6 \cos(q_3) \dot{q}_3 - \sin(q_3) \dot{q}_6 \\
 J_{d16} &= -\sin(q_3) \dot{q}_3 \\
 J_{d21} &= a l_2 \sin(q_1) \dot{q}_1 \\
 J_{d23} &= -q_6 \sin(q_3) \dot{q}_3 + \cos(q_3) \dot{q}_6 \\
 J_{d26} &= \cos(q_3) \dot{q}_3 \\
 J_{d32} &= b l_2 \cos(q_2) \dot{q}_2 \\
 J_{d34} &= -q_7 \cos(q_4) \dot{q}_4 - \sin(q_4) \dot{q}_7 \\
 J_{d37} &= -\sin(q_4) \dot{q}_4 \\
 J_{d42} &= b l_2 \sin(q_2) \dot{q}_2
 \end{aligned}$$

$$\begin{aligned}
 J_{d44} &= -q_7 \sin(q_4) \dot{q}_4 + \cos(q_4) \dot{q}_7 \\
 J_{d47} &= \cos(q_4) \dot{q}_4 \\
 J_{d51} &= a_1 \cos(q_1) \dot{q}_1 + a l_{32} \cos(q_1 + q_2) (\dot{q}_1 + \dot{q}_2) \\
 J_{d52} &= a l_{32} \cos(q_1 + q_2) (\dot{q}_1 + \dot{q}_2) \\
 J_{d55} &= -q_8 \cos(q_5) \dot{q}_5 - \sin(q_5) \dot{q}_8 \\
 J_{d58} &= -\sin(q_5) \dot{q}_5 \\
 J_{d61} &= a_1 \sin(q_1) \dot{q}_1 + a l_{32} \sin(q_1 + q_2) (\dot{q}_1 + \dot{q}_2) \\
 J_{d62} &= a l_{32} \sin(q_1 + q_2) (\dot{q}_1 + \dot{q}_2) \\
 J_{d65} &= -q_8 \sin(q_5) \dot{q}_5 + \cos(q_5) \dot{q}_8 \\
 J_{d68} &= \cos(q_5) \dot{q}_5
 \end{aligned} \tag{22}$$

When the robot hits an environment, contact force, $J^T F_e$ will react with the end effector, and this contact force is added to the dynamics.

$$M(q)\ddot{q} + C(q, \dot{q})\dot{q} = \tau + J_c^T \lambda + J^T F_e \tag{23}$$

Using (19) and (20), the dynamics of the structure can be represented as follows.

$$\begin{bmatrix} M & -J_c^T \\ -J_c & 0 \end{bmatrix} \begin{bmatrix} \ddot{q} \\ \lambda \end{bmatrix} = \begin{bmatrix} \tau - C\dot{q} + J^T F_e \\ J_c \dot{q} \end{bmatrix} \tag{24}$$

The contact forces shown previously include the Jacobian of the end effector, as in (8) and the cartesian forces, F_e acting upon contact. To include the spiral motor dynamics in the generalized closed chain model (24) has to be modified to the following.

$$\begin{bmatrix} M & 0 & -J_c^T \\ 0 & J_s & 0 \\ -J_c & 0 & 0 \end{bmatrix} \begin{bmatrix} \ddot{q} \\ \ddot{\theta} \\ \lambda \end{bmatrix} = \begin{bmatrix} \tau - C\dot{q} + J^T F_e \\ \tau_s \\ J_c \dot{q} \end{bmatrix} \tag{25}$$

The inertia terms from the angular rotation now emerges. With this modification, the d and q-axis currents could also be observed in the model. As an example, the size of the left-hand matrix becomes 17 (8 dof for biarticular structure plus 3 dof from rotational part of spiral motor and 6 dof constraints). For the biarticular muscle, J_{s1} to J_{s3} show the inertia terms from three spiral motors, thus the left hand terms of (25) can be expanded as shown.

$$\begin{bmatrix}
 M_{c11} & \dots & M_{c18} & 0 & 0 & 0 & -J_{c11} & \dots & -J_{c61} \\
 \vdots & \ddots & \vdots & \vdots & \vdots & \vdots & \vdots & \ddots & \vdots \\
 M_{c81} & \dots & M_{c88} & 0 & 0 & 0 & -J_{c18} & \dots & -J_{c68} \\
 0 & \dots & 0 & J_{s1} & 0 & 0 & 0 & \dots & 0 \\
 0 & \dots & 0 & 0 & J_{s2} & 0 & 0 & \dots & 0 \\
 0 & \dots & 0 & 0 & 0 & J_{s3} & 0 & \dots & 0 \\
 -J_{c11} & \dots & -J_{c18} & 0 & 0 & 0 & 0 & \dots & 0 \\
 \vdots & \ddots & \vdots & \vdots & \vdots & \vdots & \vdots & \ddots & \vdots \\
 -J_{c61} & \dots & -J_{c68} & 0 & 0 & 0 & 0 & \dots & 0
 \end{bmatrix} \tag{26}$$

and

$$[\ddot{q}_1 \dots \ddot{q}_8 \quad \ddot{\theta}_1 \quad \ddot{\theta}_2 \quad \ddot{\theta}_3 \quad \ddot{\lambda}_1 \quad \dots \quad \ddot{\lambda}_6]^T$$

The right hand term of (25) can be expanded as shown.

$$\begin{bmatrix} \tau_1 \\ \vdots \\ \tau_8 \end{bmatrix} - \begin{bmatrix} C_{11} & \dots & C_{18} \\ \vdots & \ddots & \vdots \\ C_{81} & \dots & C_{88} \end{bmatrix} \begin{bmatrix} \dot{q}_1 \\ \vdots \\ \dot{q}_8 \end{bmatrix} + J^T F_e \begin{bmatrix} K_{\tau_1} I_{q1} - h_1(K_{f1} I_{d1} + K_{g1} x_{g1}) \\ K_{\tau_2} I_{q2} - h_2(K_{f2} I_{d2} + K_{g2} x_{g2}) \\ K_{\tau_3} I_{q3} - h_3(K_{f3} I_{d3} + K_{g3} x_{g3}) \\ J_{d11} & \dots & J_{d18} \\ \vdots & \ddots & \vdots \\ J_{d61} & \dots & J_{d68} \end{bmatrix} \begin{bmatrix} \dot{q}_1 \\ \vdots \\ \dot{q}_8 \end{bmatrix} \quad (27)$$

From $[q_6, q_7, q_8]^T$ and $[\theta_1, \theta_2, \theta_3]^T$, the gaps can be obtained by (28) and similarly for velocity and acceleration.

$$\begin{bmatrix} x_{g1} \\ x_{g2} \\ x_{g3} \end{bmatrix} = \begin{bmatrix} q_6 - h\theta_1 \\ q_7 - h\theta_2 \\ q_8 - h\theta_3 \end{bmatrix} \quad (28)$$

The environment interacting with the end effector could be represented in terms of impedance (with stiffness K_e and damping D_e).

$$F_e = K_e X_o + D_e \dot{X}_o \quad (29)$$

Different environment will incur different values of stiffness and damping, i.e. stiffness of a concrete wall is greater than the stiffness of a rubber ball. The illustration of the biarticular structure in contact with the environment is shown in Fig. 11.

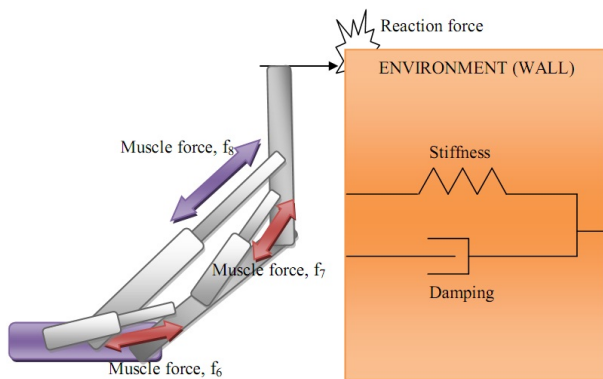


Fig. 11. Illustration of Biarticular Manipulator with Environment

6 FORCE CONTROL SCHEME FOR BIARTICULAR MANIPULATOR

Position control is sufficient for tasks which do not involve interaction with any objects or environment, for example spray-painting for cars in a factory line, and also workspace which has proper fence surrounding the robot (no human interference during operation). In the case of position control in the presence of environment, undesirably large forces would be applied as soon as the end effector contacts the environment to overcome the obstacle in order to reach the desired trajectories designed.

In the presence of human, safe and compliant control is highly required to avoid damage to human/environment. This is important in human-robot interaction/co-operation. Small deviations in position are acceptable, as long as the forces are maintained not to exceed certain values (that could injur/harm human or environment), hence the term force control.

For a robotic manipulator, the forces that need to be controlled are the end effector or tool position. The biarticular manipulator would also require the end effector to be controlled in cartesian space and then the forces in cartesian converted to forces in muscle actuation. Although the forces controlled are in the muscle domain, the equivalent virtual torques in the shoulder and elbow could be obtained by using the muscle to joint jacobian. This property is important, because it does not make the control difficult, instead contributes to simplifications of the model.

The force control scheme for the actuation-redundant biarticular manipulator could be represented as in Fig. 12. It can be seen that the force control scheme involves the use of disturbance observers to estimate the reaction forces in the cartesian domain. The cartesian velocities could be obtained from virtual joint velocities using conventional jacobian terms. Force reference command is labeled as F_{cmd} , a vector of x-direction and y-direction force references. K_e is the vector of force control gain for x and y.

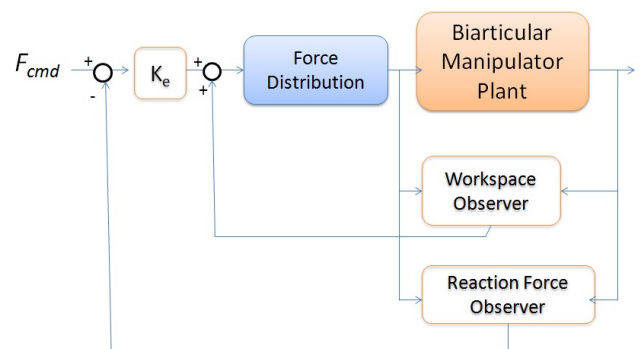


Fig. 12. Force Control Scheme for Biarticular Manipulator

In Fig. 12, force distribution block is shown in the control. This is because the end effector forces (in x and y-direction) need to be converted to the muscle forces for shoulder monoarticular, elbow monoarticular and biarticular muscle which will be tracked by muscle-level control. In short, the muscle forces are obtained by using the conventional jacobian transpose with the muscle jacobian, in other words, reversing (9).

$$F_{lmq} = [J_{lmq}^T]^{-1} J^T F_e \quad (30)$$

Since the muscle jacobian is non-square, the Moore's pseudo inverse matrix is used for inversion.

$$[J_{lmq}^T]^{-1} = [J_{lmq}][J_{lmq}^T J_{lmq}]^{-1} \quad (31)$$

Next, the workspace observer is designed. This is because the measurable variables are from the spiral motors (linear and rotational displacements) and there are no encoders on the elbow and shoulder joints. However, the angles can be calculated from the muscle kinematics shown earlier.

$$q_1 = \cos^{-1} \left(\frac{l_{m1}^2 - a l_1^2 - a l_2^2}{2 a l_1 a l_2} \right) \quad (32)$$

$$q_2 = \cos^{-1} \left(\frac{l_{m2}^2 - b l_1^2 - b l_2^2}{2 b l_1 b l_2} \right) \quad (33)$$

For the angle velocities, these can be obtained by the following equation.

$$\begin{bmatrix} \dot{q}_1 \\ \dot{q}_2 \end{bmatrix} = J_{lmq}^{-1} \begin{bmatrix} \dot{l}_{m1} \\ \dot{l}_{m2} \\ \dot{l}_{m3} \end{bmatrix} \quad (34)$$

Then the end effector position and velocities can be obtained via two-link forward kinematics and jacobian.

$$\begin{bmatrix} x \\ y \end{bmatrix} = \begin{bmatrix} a_1 \cos(q_1) + a_2 \cos(q_1 + q_2) \\ a_1 \sin(q_1) + a_2 \sin(q_1 + q_2) \end{bmatrix} \quad (35)$$

$$\begin{bmatrix} \dot{x} \\ \dot{y} \end{bmatrix} = \begin{bmatrix} J_{11} & J_{12} \\ J_{21} & J_{22} \end{bmatrix} \begin{bmatrix} \dot{q}_1 \\ \dot{q}_2 \end{bmatrix} \quad (36)$$

And end effector forces derived from muscle forces are again shown.

$$\begin{bmatrix} F_x \\ F_y \end{bmatrix} = [J^T]^{-1} J_{lmq}^T \begin{bmatrix} F_{lm1} \\ F_{lm2} \\ F_{lm3} \end{bmatrix} \quad (37)$$

Then the estimated outputs of the workspace observer (x and y disturbance) can then be constructed.

$$\hat{f}_x = \frac{g_{fx}}{s + g_{fx}} (F_x + g_{fx} M_x \dot{x}) - g_{fx} M_x \dot{x} \quad (38)$$

$$\hat{f}_y = \frac{g_{fy}}{s + g_{fy}} (F_y + g_{fy} M_y \dot{y}) - g_{fy} M_y \dot{y} \quad (39)$$

For the reaction force observer block, the same inputs are taken from the manipulator plant (i.e. muscle length, velocities). However, the outputs are slightly different than the workspace observer because it takes into account the estimated centrifugal/coriolis forces (C terms) as shown in the following equations.

$$\hat{f}_{rx} = \hat{f}_x - C_{11}(J_{11}\dot{q}_1 + J_{12}\dot{q}_2) \quad (40)$$

$$\hat{f}_{ry} = \hat{f}_y - C_{22}(J_{21}\dot{q}_1 + J_{22}\dot{q}_2) \quad (41)$$

Until this point, force control in taskspace was derived. However, these muscle forces will become reference forces for the muscle-level control to track. This is due to the equations of motion of the spiral motor. For the muscle-level control, the block diagram in Fig. 13 shows the overall scheme. At this level, force tracking and gap control is performed simultaneously. Linear and rotational disturbance observers are estimated from the two degree-of-freedom plant model shown in (10) and (11). Dq-axis current references are generated to control the spiral motor actuation. The next step is d-q axis current tracking by the PI controller which is fed into the three-phase Permanent Magnet spiral motor (shown as 2 dof Spiral Motor plant). The power used for driving the manipulator structure can be obtained from the d- and q-axis currents because the spiral motor is a Permanent Magnet motor. Accordingly energy utilized can be obtained.

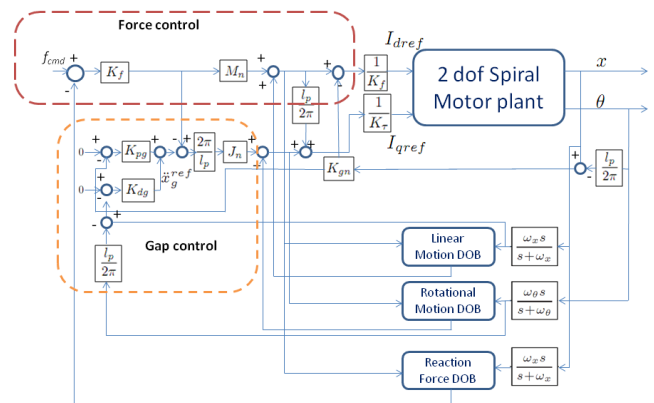


Fig. 13. Force Control Scheme for a Spiral Motor

The linear motion and rotational motion disturbance observers can be estimated by the Equations (42) and (42).

The reaction force observer is almost similar to linear motion disturbance observer but added with a constant friction term D_x which is arbitrarily chosen.

$$\begin{aligned} \hat{d}_x &= \frac{g_x}{s + g_x} (K_{fn} I_{dref} + K_g x_g + g_x M_n \dot{x}) - g_x M_n \dot{x} \\ \hat{d}_\theta &= \frac{g_\theta}{s + g_\theta} (K_\tau I_{qref} - h(K_f I_d + K_g x_g) + g_\theta J_n \dot{\theta}) - g_\theta J_n \dot{\theta} \end{aligned} \quad (42)$$

The difference between force control for the conventional two-link manipulator and force control for the biarticular manipulator is the muscle Jacobian term. If the number of muscles used is multiplied, computational cost of the muscle Jacobian will increase. For example, structures with 6 muscles from the shoulder to the elbow would incur heavier computation than 3 muscle structure.

6.1 Independent Muscle Control

For independent force control of each muscles, the interaction with the environment will be investigated. The initial position of the end effector was set at (0.15, 0.53) m. The environment is set at x-position of 0.16. Stiffness and damping values of the environment are 3000 and 20. Although these parameters are set, the disturbance observer force control scheme is robust and can work in unknown or unstructured environments as well. Simulation is performed in two types of structure; structure with monoarticular muscles only and structure with monoarticular and biarticular muscles. Force commands were set at 10 N at $t = 0.5$ s for each muscles. Before $t = 0.5$ s, the gap magnetic levitation is realized. The detail description of force control for spiral motors can be referred to in [33]. Comparison between the x trajectories of both structure can be seen in Fig. 14 while gap responses are shown in Fig. 15.

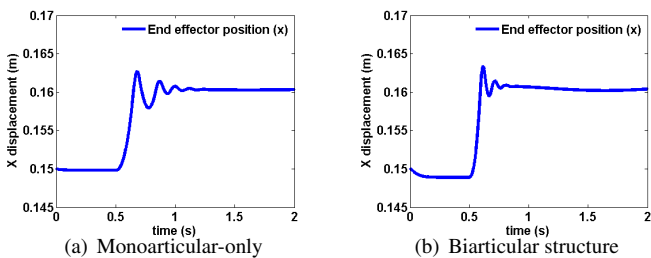


Fig. 14. Independent muscle control: X displacements

It can be seen that collision between monoarticular-only manipulator and the environment occurs at $t = 0.68$ s while the biarticular manipulator collides with the environment faster, at $t = 0.60$ s. This is due to the additional actu-

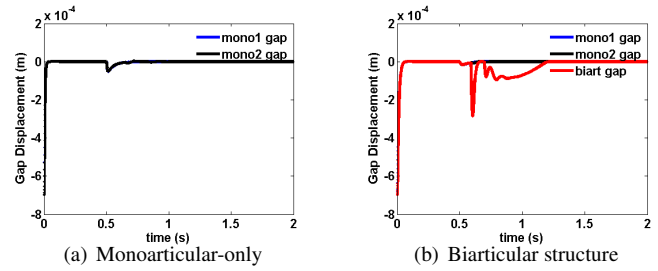


Fig. 15. Independent muscle control: Gap displacements

ation from biarticular muscle which induces faster performance. However, the gap responses of the biarticular muscle vary relatively larger than monoarticular gap responses (red line in Fig. 15).

Fig. 16 shows the muscle forces and end effector forces for the monoarticular structure.

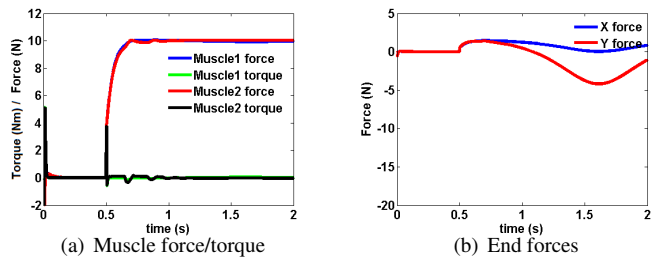


Fig. 16. Independent muscle control: forces for monoarticular

The force control of independent muscles was successfully achieved in the monoarticular structure. The end effector forces vary between 1.5 N to -4.5 N because the end effector position changes (slides).

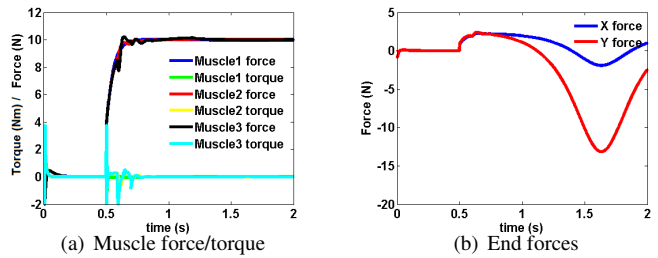


Fig. 17. Independent muscle control: biarticular forces

For the biarticular muscle (Fig. 17), although the force responses are twice faster than monoarticular structure, there is an obvious interaction between the monoarticular 2 (elbow) muscle and the biarticular muscle. This is from the

actuation redundancy on the elbow angle for both monoarticular 2 and biarticular muscle. However, after 0.75s, each muscle forces stabilize. The end effector forces are between 2.5 N to -15 N due to sliding at the environment surface. The dq currents are shown in Fig. 18 and Fig. 19.

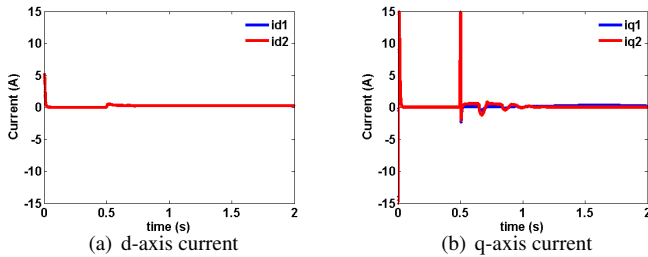


Fig. 18. Independent muscle control: monoarticular currents

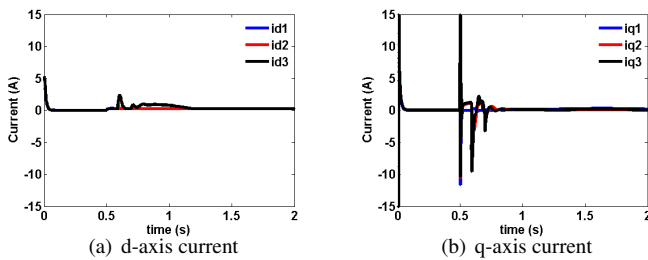


Fig. 19. Independent muscle control: biarticular currents

6.2 End Effector Muscle Control

Using the same initial position and environmental parameters, the muscle forces are indirectly controlled by the end effector forces in the cartesian domain. Initially, the end effector force in proper direction is given to ensure that the end effector hits the environment. After contacting with the environment, the forces are controlled to maintain end effector forces in the x-direction.

The force reference in the x-direction is given as 10 N and force reference for y-direction is 0 N. X-direction trajectory is shown in Fig. 20 and its gap responses depicted in Fig. 21.

Collision for biarticular structure occurs faster than monoarticular structure. The forces for the monoarticular-only structure is shown in Fig. 22.

As seen in Fig. 22, the end effector forces in x-direction were tracked, initially with overshoot. Also, y end forces are maintained at 0 N. This is achieved by monoarticular 1 (shoulder) force of 100 N and lesser force of 60 N from monoarticular 2 (elbow) muscle.

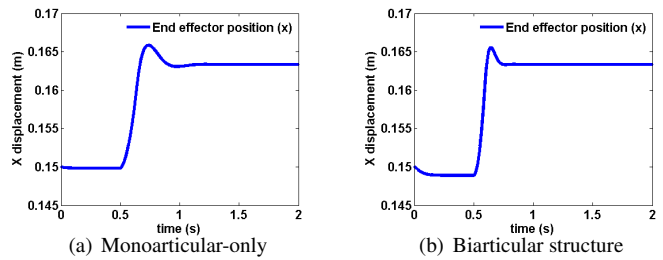


Fig. 20. End effector step force control: X displacements

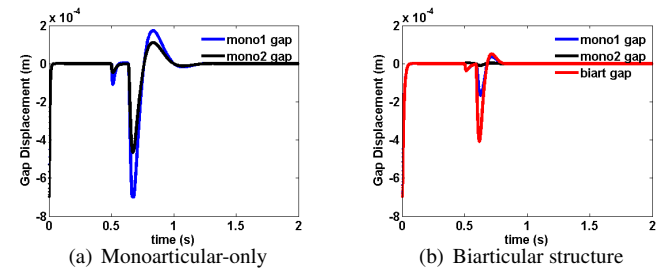


Fig. 21. End effector step force control: Gaps

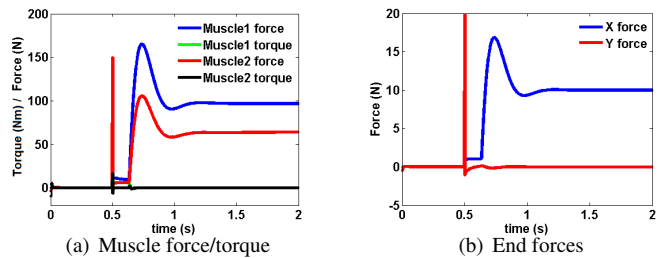


Fig. 22. End effector step force control: Monoarticular forces

For the biarticular structure case, as shown in Fig. 23, the end effector forces were also tracked successfully with the biarticular structure settling faster than the monoarticular structure. However, there were overshoots in the x-direction force and fluctuations in the y-direction force during collision. After collision, both forces stabilized with x force at 10 N and y force at 0 N. The main advantage of the biarticular manipulator compared to monoarticular manipulator is the reduced muscle forces required to track the force command. The existence of biarticular muscles reduces the effort of the elbow monoarticular muscle.

The actuation redundancy in the manipulator shows no problem in actuation due to the efficient force distribution via the product of the conventional jacobian and muscle jacobian which was previously shown in (30).

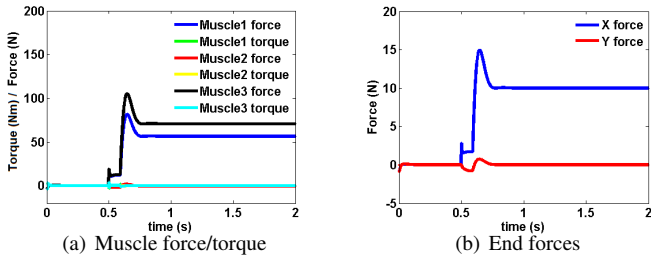


Fig. 23. End effector step force control: biarticular forces

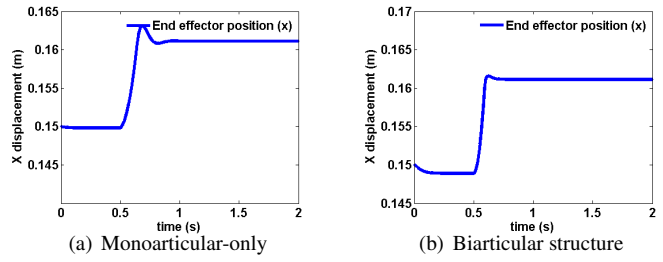


Fig. 26. Musculoviscoelasticity control: X displacements

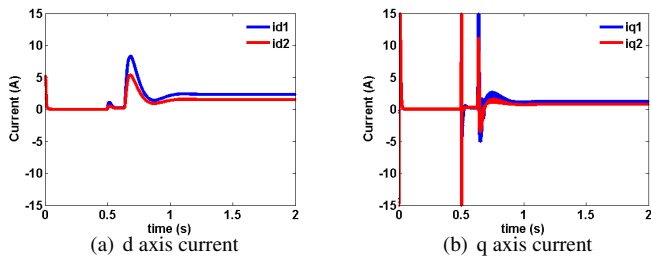


Fig. 24. End effector control: monoarticular currents

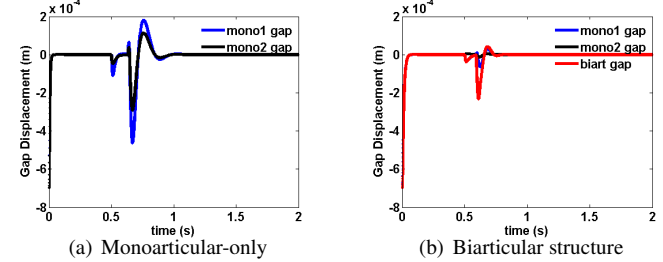


Fig. 27. Musculoviscoelasticity control: Gaps

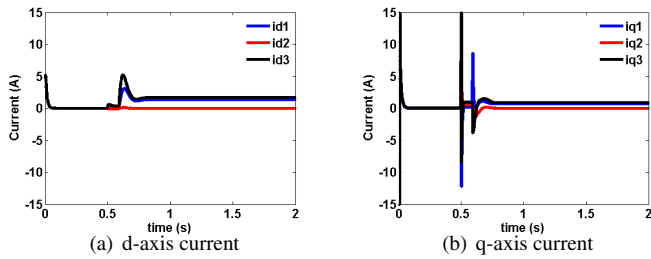


Fig. 25. End effector control: biarticular currents

6.3 Muscular Viscoelasticity Control

The control goal of this part is to assess the spiral motor redundant-actuator performance in the case of muscular force control. This control scheme is to emulate muscular viscoelasticity [34] by applying the following force command;

$$f^{cmd} = (u_e - u_f) + (u_e + u_f)(K_m(x_0 - x) - D_m \dot{x}) \quad (43)$$

where u_e and u_f are contractile force of virtual extensor and flexor muscles respectively. K_m and D_m values are set as 10% of the environmental values. Due to the ability of the spiral motor to generate both pulling and pushing force, a single spiral motor is sufficient to emulate an antagonistic muscle pair.

Linear and gap displacements for monoarticular-only structure and biarticular structure can be seen in Figures

26 and 27. For the monoarticular structure, the force responses are shown in Fig. 28.

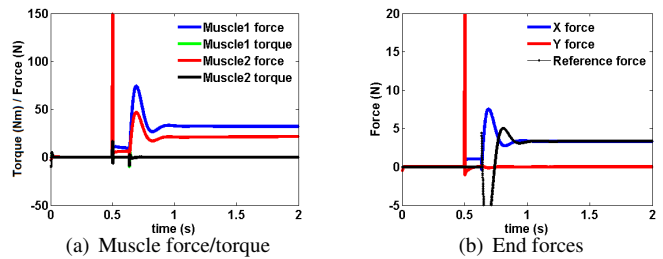
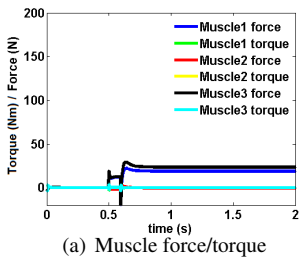


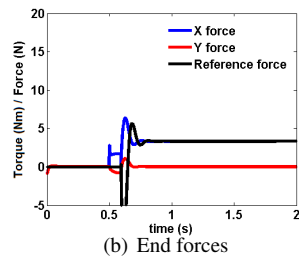
Fig. 28. Musculoviscoelasticity forces: monoarticular

From the force responses of monoarticular muscles (Fig. 28), the muscular viscoelasticity tracks the force successfully, with overshoots. This is done by forces of monoarticular muscles of around 30 N for monoarticular 1 (shoulder) and 20 N for monoarticular 2 (elbow). Y-Force was also stable at 0 N towards the end.

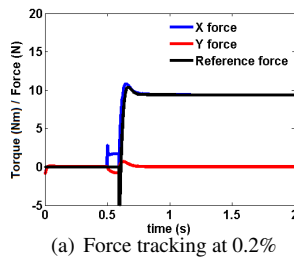
From the responses of the biarticular forces (Fig. 29), end effector forces were also tracked successfully. The overshoots were significantly lower than monoarticular structure and the end forces of biarticular structure were achieved using significantly less amount of forces from monoarticular 2. Biarticular force of around 24 N and monoarticular force of 19 N were used. Currents are shown in Figs 30 and 31.



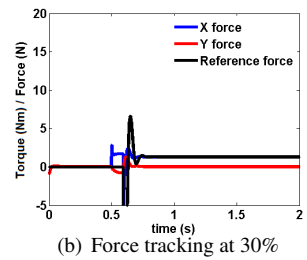
(a) Muscle force/torque



(b) End forces



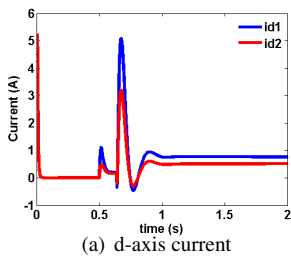
(a) Force tracking at 0.2%



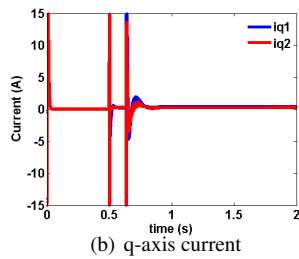
(b) Force tracking at 30%

Fig. 29. Musculoviscoelasticity forces: biarticular

Fig. 32. Musculoviscoelasticity forces at 0.2% and 30%: biarticular

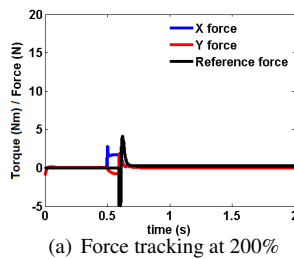


(a) d-axis current

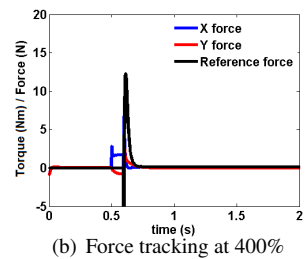


(b) q-axis current

Fig. 30. Musculoviscoelasticity currents: monoarticular

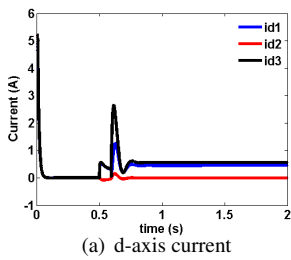


(a) Force tracking at 200%

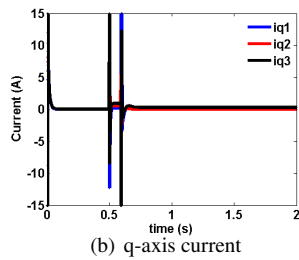


(b) Force tracking at 400%

Fig. 33. Musculoviscoelasticity forces at 200% and 400%: biarticular

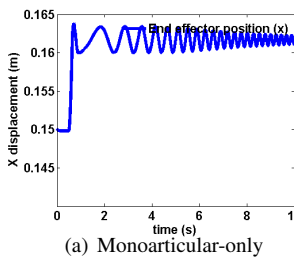


(a) d-axis current

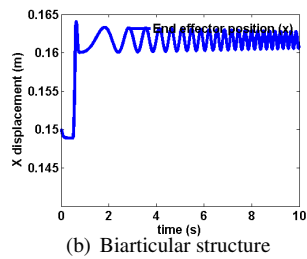


(b) q-axis current

Fig. 31. Musculoviscoelasticity currents: biarticular



(a) Monoarticular-only



(b) Biarticular structure

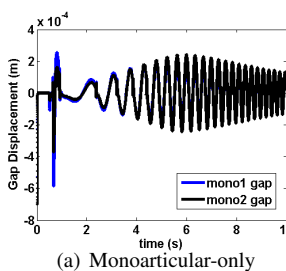
Fig. 34. Varying force reference: X displacements

To demonstrate that our controller is robust even with varying gains (or unknown environment parameters), we will show the musculoviscoelasticity control results with variations of K_m and D_m with 0.2%, 30%, 200% and 400%. In all cases (refer Figs 32 and 33), the biarticular structure could track the force references.

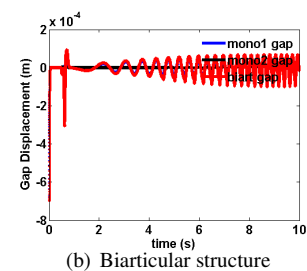
6.4 End effector control with varying force reference

This section investigates the effect of varying frequency of force reference for the musculoskeletal manipulator. Force reference was generated using sinusoidal waveform with increasing frequency. We extend the simulation time from 2 seconds to 10 seconds. Fig. 34 shows the end effector x displacement. The changing position of the object is due to sinusoidal force command shown in Equation (44) (with A as the force magnitude).

$$f^{cmd} = A(0.5(1 - \cos 2\pi t^2)) \quad (44)$$



(a) Monoarticular-only



(b) Biarticular structure

Fig. 35. Varying force reference: Gaps

As seen in Fig. 35, the gaps were maintained within limits for both monoarticular and biarticular structure. Monoarticular structure shows larger oscillations compared to biarticular.

For muscle forces used to track the end effector (refer Fig. 36), larger forces were required for monoarticular structure than biarticular (refer Fig. 37). Also, monoarticular end effector hits the environment several times as seen in the sparks in end effector forces.

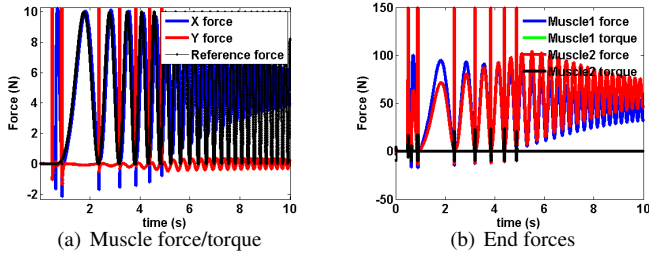


Fig. 36. Varying force: monoarticular structure forces

At low frequencies, force reference was tracked successfully. But as frequencies increases, the manipulator could not achieve the desired force but tracks the forces with slightly lower force magnitude.

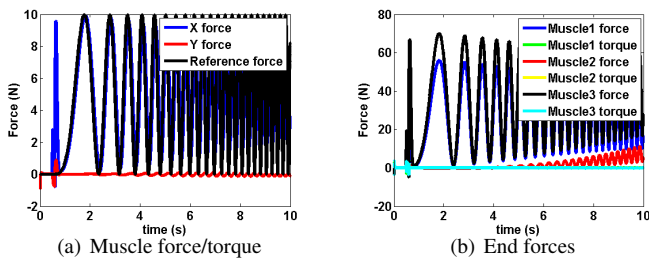


Fig. 37. Varying force: biarticular structure forces

D-axis current of biarticular manipulator (refer Fig. 39) shows lower magnitude than monoarticular manipulator d-axis current (refer Fig. 38).

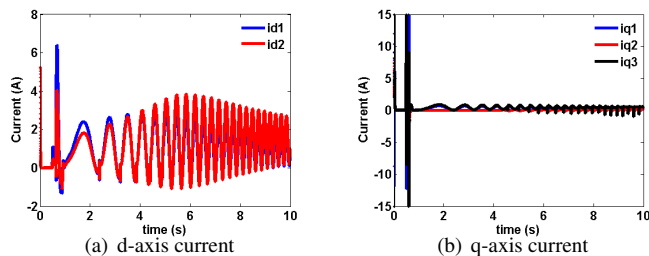


Fig. 38. Varying force: monoarticular structure currents

7 SUMMARY

This paper addresses force control of musculoskeletal manipulator in the presence of environmental contact.

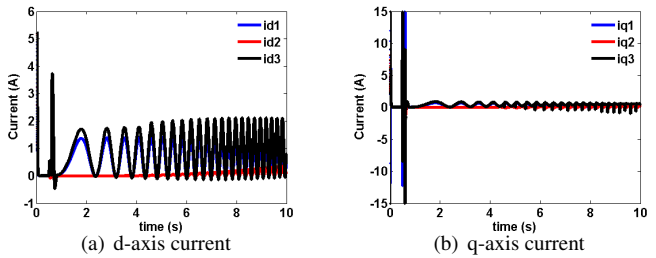


Fig. 39. Varying force: biarticular structure currents

By using disturbance observers designed in workspace and muscle-space, force control were simulated in three different schemes, independent muscle control, step force command and muscular viscoelasticity control.

Some significant advantages of the biarticular manipulator were the faster responses in the independent muscle force control, reduced force overshoot in step force command and efficient force distribution (reduction of monoarticular muscle burden) in the end effector step force commands and muscular viscoelasticity control.

The feasibility of force control on biarticular manipulator shows the uniqueness of the human arm structure that could be further explored for more advanced applications in robotics. Although the results shown were for the spiral motor based structure, the force control scheme can generally be applied to other prismatic motors, i.e tubular linear motors. However the main significant of this paper is the ability to maintain gap control for the spiral motors throughout all the force schemes. This work was supported by KAKENHI 24246047.

REFERENCES

- [1] M. Hirose, K. Ogawa, "Human humanoid robots development," Phil. Trans. R. Soc. A, 365, pp 11-19, 2007.
- [2] Sami Haddadin, Simon Haddadin, A. Khoury, T. Rokahr, S. Parusel, R. Burgkart, A. Bicchi, A. Albu-Schäffer "On Making Robots Understand Safety I: Embedding Injury Knowledge into Control", accepted for publication: International Journal of Robotics Research, 2012.
- [3] M. Malchano, K. Blankespoor, A. Howardy, A.A. Rizzi, M. Raibert, "Autonomous navigation for Big-Dog," International Conference on Robotics and Automation, pp 4736 - 4741, May 2010.
- [4] H. Asada and T. Kanade, "Design of direct-drive mechanical arms," Trans. ASME, J. Vib. Acoust. Stress Reliab. Des., vol. 105, no. 3, pp. 312–316, 1983.

- [5] T. Murakami, F. Yu, and K. Ohnishi, "Torque sensorless control in multidegree-of-freedom manipulator," *IEEE Trans. Ind. Electron.*, vol. 40, no. 2, pp. 259–265, Apr. 1993.
- [6] S. Katsura, Y. Matsumoto, and K. Ohnishi, "Analysis and experimental validation of force bandwidth for force control," *IEEE Trans. Ind. Electron.*, vol. 53, no. 3, pp. 922–928, Jun. 2006.
- [7] S. Katsura, K. Irie, and K. Ohnishi, "Wideband force control by position acceleration integrated disturbance observer," *IEEE Trans. Ind. Electron.*, vol. 55, no. 4, pp. 1699–1706, Apr. 2008.
- [8] C. Mitsantisuk, S. Katsura, and K. Ohishi, "Force control of human–robot interaction using twin direct-drive motor system based on model space design," *IEEE Trans. Ind. Electron.*, vol. 57, no. 4, pp. 1383–1392, Apr. 2010.
- [9] G. Pratt and M. Williamson, "Series elastic actuators," in *Proc. IEEE/RSJ IROS*, pp. 399–406, 1995.
- [10] K. Abe, T. Suga, Y. Fujimoto, "Control of a Biped Robot Driven By Elastomer-based Series Elastic Actuator", *IEEE Int. Workshop on Advanced Motion Control*, 978-1-4577-1073-5/12, Mar. 2012.
- [11] T.Y. Choi, J.J. Lee, "Control of Manipulator using Pneumatic Muscles for Enhanced Safety", *IEEE Transactions on Industrial Electronics*, Vol. 57, no. 8, pp.2815-2285, August 2010.
- [12] K. Hosoda, H. Takayama, T. Takuma "Bouncing Monopod with Bio-mimetic Muscular-Skeleton System", *International Conference on Intelligent Robots and Systems*, pp.3083-3088, Sept 2008.
- [13] R. Niiyama, A. Nagakubo, Y. Kuniyoshi "Mowgli: A Bipedal Jumping and Landing Robot with an Artificial Musculoskeletal System", *International Conference on Robotics and Automation*, pp.2546-2551, April 2007.
- [14] H. Tomori, Y. Midorikawa, T. Nakamura, "Derivation of Nonlinear Dynamic Model of Novel Pneumatic Artificial Muscle Manipulator with a Magnetorheological Brake," *IEEE Int. Workshop on Advanced Motion Control*, 978-1-4577-1073-5/12, Mar. 2012.
- [15] D.B.Reynolds, D.W.Repperger, C.A. Phillips, G. Bandry "Modeling the dynamic characteristics of pneumatic muscle", *Annals of Biomedical Engineering*, Springer, Vol. 31, pp.310-317, January 2003.
- [16] T. Boaventure, C. Semini, J. Buchli, M. Frigerio, M. Focchi, D.G. Caldwell "Dynamic Torque Control of a Hydraulic Quadruped Robot", *IEEE Int. Conf. on Robotics and Automation*, pp.1889-1894, May 2012.
- [17] Raytheon Company: XOS 2 Exoskeleton, http://www.raytheon.com/newsroom/technology/rtn08_exoskeleton/.
- [18] S. Oh, Y. Hori "Development of Two-Degree-of-Freedom Control for Robot Manipulator with Biarticular Muscle Torque", *American Control Conference*, pp.325-330, July 2009.
- [19] V. Salvucci, Y. Kimura, S. Oh, Y. Hori, "BiWi: Bi-Articularly Actuated and Wire Driven Robot Arm", *The IEEE International Conference on Mechatronics*, pp.827-832, April 2011.
- [20] T. Tsuji, "A Model of Antagonistic Triarticular Muscle Mechanism for Lancelet Robot", *The 11th IEEE International Workshop on Advanced Motion Control*, pp.496-501, March 2010.
- [21] Y. Muraguchi, M. Karita, H. Nakagawa, T. Shinya, and M. Maeda, "Method of measuring dynamic characteristics for linear servo motor and comparison of their performance," in *Proc. LDIA*, pp. 204–207, 1998
- [22] N. Bianchi, S. Bolognani, D. D. Corte, and F. Tonel, "Tubular linear permanent magnet motors: An overall comparison," *IEEE Trans. Ind. Appl.*, vol. 39, no. 2, pp. 466–475, Mar. 2003
- [23] L. Norum, R. Nilssen, "Analysis of tubular linear permanent magnet motor for drilling application," *IEEE Int. Conf. on Electric Power and Energy Conversion Systems*, pg 1-5, Nov. 2009
- [24] Y. Ye, Z. Zheng, Q. Lu, "A novel tubular permanent magnet linear synchronous motor used for elevator door," *IEEE Int. Conf. on Electrical Machines and Systems ICEMS*, pg 801-804, Oct. 2007.
- [25] Y. Fujimoto, T. Kominami, H. Hamada "Development and Analysis of a High Thrust Force Direct-Drive Linear Actuator", *IEEE Transactions on Industrial Electronics* Vol.56, No.5, pp 1383-1392, May 2009.
- [26] I.A. Smadi, H. Omori, Y. Fujimoto, "On Independent Position/Gap Control of a Spiral Motor", *The 11th IEEE International Workshop on Advanced Motion Control*, pp 478-483, March 2010.
- [27] I.A. Smadi, H. Omori, Y. Fujimoto, "Development, Analysis and Experimental Realization of a Direct-Drive Helical Motor", *IEEE Transactions on Industrial Electronics*, Vol. 59, No. 5, pp 2208-2216, May 2012.

- [28] A.Z.Shukor, Y. Fujimoto, "Development of a Biarticular Manipulator using Spiral Motors", The 37th Annual Conference of the IEEE Industrial Electronics Society, November 2011.
- [29] A.Z.Shukor, Y. Fujimoto, "Workspace Control of Biarticular Manipulator", The IEEE International Conference on Mechatronics, pp.415-420, April 2011.
- [30] F.H. Ghorbel, O. Chetelat, R. Gunawardana, R. Longchamp, "Modeling and Set Point Control of Closed-Chain Mechanisms: Theory and Experiment", International Transactions on Control Systems Technology Vol. 8, no. 5, pp 801-814, September 2000.
- [31] Y. Nakamura, M. Ghodoussi "Dynamics Computation of Closed-Link Robot Mechanisms with Nonredundant and Redundant Actuators", IEEE Transactions on Robotics and Automation Vol. 5, no. 3, pp 294-302, June 1989.
- [32] M.W. Spong, M. Vidyasagar, "Robot Dynamics and Control", John Wiley and Sons, pp 23-24, 1989.
- [33] Y. Fujimoto, I. A. Smadi, H. Omori, Y. Wakayama, "High Thrust Force Direct-Drive Linear Actuator and Its Application to Musculoskeletal Robots", Proceedings of the International Symposium on Application of Biomechanical Control Systems to Precision Engineering (ISAB), pp. 217-222, July 2010.
- [34] K. Ito, T. Tsuji, "The Bilinear Characteristics of Muscle-Skeletomotor System and the Application to Prosthesis Control", Transactions of the Electrical Engineers of Japan, vol. 105-C, no. 10, pp 201-208, 1985.



Ahmad Zaki Shukor received the B.E. from Universiti Teknologi Malaysia in 2002 and M.E. from University of South Australia in 2004. He is currently pursuing in PhD in Yokohama National University, Japan. From 2002, he is attached to Universiti Teknikal Malaysia Melaka. His research interests include actuators, robotics, and motion control. Ahmad Zaki Shukor is a graduate member of the Board of Engineers Malaysia and Robotics Society of Japan.



Yasutaka Fujimoto received the B.E., M.E., and Ph.D. degrees in electrical and computer engineering from Yokohama National University, Yokohama, Japan, in 1993, 1995, and 1998, respectively. In 1998, he joined the Department of Electrical Engineering, Keio University, Yokohama, Japan, as a Research Associate. Since 1999, he has been with the Department of Electrical and Computer Engineering, Yokohama National University, where he is currently an Associate Professor. His research interests include actuators, robotics, manufacturing automation, and motion control. Dr. Fujimoto is a member of the IEEE Industrial Electronics Society Technical Committee on Sensors and Actuators, Institute of Electrical Engineers of Japan, and Robotics Society of Japan.

AUTHORS' ADDRESSES

**Ahmad Zaki bin Hj Shukor, MEng,
Assoc. Prof. Yasutaka Fujimoto, Ph.D.,
Department of Electrical and Computer Engineering,
Faculty of Engineering,
Yokohama National University,
79-5 Tokowadai, Hodogaya-ku, Yokohama 240-8501,
Japan
email: zaki@fujilab.dnj.ynu.ac.jp,
fujimoto@ynu.ac.jp**

Received: 2012-06-29

Accepted: 2012-10-17